Iranian Journal of Materials Forming 7 (2) (2020) 88-103

Online ISSN: 2383-0042

IJMF

Iranian Journal of Materials Forming

Journal Homepage: http://ijmf.shirazu.ac.ir

Research Article

Structural Mechanics Approach to Investigate the Hyperelastic Mechanical Behavior of Single and Multi-wall Carbon Nanotubes

M. Rashidi and K. Narooei*

Department of Materials Science and Engineering, K. N. Toosi University of Technology, Tehran, Iran

ARTICLE INFO

Article history:

Received 25 July 2020
Revised 10 October 2020
Accepted 12 October 2020

Keywords:

SWCNT
MWCNT
Hyperelastic
Brenner potential
Lennard Jones potential

ABSTRACT

In the current research, a three-dimensional finite element model was considered to predict the mechanical behavior of Single Wall (SWCNTs) and Multi Wall Carbon Nanotubes (MWCNTs). Assuming the nonlinear elastic behavior of C-C bond in large strains, hyperelastic models were considered. Literature review revealed that the material parameters of the hyperelastic models have been determined from the uniaxial tension loading, although the nonlinear elastic behavior is not identical in the tension and compressions. Thereby, the energy-stretch curve of C-C bond was determined from the second-generation Brenner potential in uniaxial tension and compression conditions. The results were fitted to the Ogden, Moony-Rivlin, and Yeoh hyperelastic strain energy functions to derive the material parameter of the mentioned models. The results indicated that the second order Ogden model could describe the tensile and compressive hyperelastic behavior of the C-C bonds accurately. The results of SWCNT bending showed that a unique response could be captured by considering the tension and compression simultaneously in deriving of the material parameters. From the results of SWCNT, the mechanical behavior of MWCNTs were predicted by assuming the Van der Waals bonds between the layers using the Lennard-Jones potential. Results of loading on the external layer of MWCNTs showed that an increase in the layers causes a decrease in the stress so that the stress-strain curves become identical beyond 8 layers. Accordingly, the material parameters of the first order Ogden model were determined for MWCNTs considering the simultaneous response in tension and compression.

1. Introduction

Carbon nanotubes (CNTs) have been used in many applications including composite materials, due to their high stiffness, strength, and flexibility in addition to their low density [1]. As an example, the CNTs were used in production of carbon nanotube sponges by chemical vapor deposition method and some excellent properties like oil absorbent, low density, and large elastic deformation could be mentioned [2]. The oilphilic property of these materials has presented them as oil absorbent materials and the absorbed organic materials could be removed by application of low amounts of pressure or burning of carbon nanotube sponges [3].

During recent decades, some extensive empirical and computational studies have been carried out to clarify the mechanical properties of CNTs. However, due to the dispersed data resulting from the empirical findings which have been influenced by some factors including ambient conditions, tool precision, and defects of the CNTs structure, the experimental techniques are under constraints [4]. Thus, other methods were employed such as atomistic modeling, continuum model, and nano-

* Corresponding author
E-mail address: knarooei@kntu.ac.ir (K. Narooei)

scale continuum modeling. Atomistic modeling includes the molecular dynamic method, Monte Carlo technique, and Ab initio approximation where the molecular dynamic method has been widely used. However, in these methods the time and dimensions should be limited due to the high computational cost. By neglecting the atomic bonds, the continuum technique provides a potential for simulation in larger scales. But, as a result of neglecting the chirality and atomic structure, this method is also under criticism. However, the nano-scale continuum modeling technique that is implemented by Finite Element Method (FEM) provides possible simulation of CNT with spring, truss, and beam elements. In this method, various loading modes such as tension, compression, and shear are imposed on the C-C bond to obtain the mechanical behavior of a bond using chemical potential functions and arrangement of carbon atoms along each other in CNT [5].

Many researches have been so far implemented about the mechanical behavior of CNTs under various loading conditions. Tserpes et al. [6] determined the effect of the CNT diameter on the Young modulus of SWCNT, assuming relation between the molecular and structural mechanics. They found that the Young modulus of SWCNT may remain fixed despite an increase in the diameter. Xiao et al. [7] used the molecular dynamic method and the second-generation Brenner potential [8] to obtain the mechanical behavior of (10, 10) SWCNT and they found that the stress-strain response becomes nonlinear in large strains. Wen Xing et al. [9] obtained similar result to Xiao et al. [7] and they mentioned that the chirality has no effect on the Young modulus of SWCNTs. Dilrukshi et al. [10] explored the mechanical behavior of armchair and zigzag SWCNTs and they found the influence of potential field is much higher in the torsional behavior. Liang et al. [11] used the semi-moment theory and molecular dynamics simulations to describe the bending behavior of SWCNTs. Their results showed that the zigzag SWCNTs with length-to-diameter ratio of 2.35∼14.11 and the armchair SWCNTs with length-to-diameter ratio of 2.41∼12.39 represent similar behavior. Ling et al. [12, 13] compared the energy-strain curve of (10, 10) SWCNT with the results given by Xiao et al. [7] and they found that CNTs represent the hyperelastic behavior and their behavior may not be obtained accurately by linear equations. Likewise, Flores et al. [14] derived the material parameters of the first order Ogden model [15] to describe the CNTs buckling using the relationship among the molecular and structural mechanics. Flores et al. [16] obtained the energy-stretch curve for the C-C bond using the Tersoff-Brenner potential [17] in the Material Studio software and concluded that bond breaking occurs at the strain level of 0.33. Afterwards, in regards to the nonlinearity of the resulting curve and adjusting it to the first order Ogden model, they studied the nonlinear behavior of the armchair SWCNTs under tensile loading. They found two distinct sets of the material parameters for tension and compression. However, Darijani and Naghdabadi [18] and Hosseinzadeh et al. [19] mentioned that the material parameters of the hyperelastic models should be obtained from coupling of different basic loading modes. Kalamkarov et al. [20] calculated the Young and shear modulus of SWCNTs, armchair, and zigzag MWCNTs using the second-generation Brenner potential [8] for the C-C bond behavior and the Lennard-Jones potential [21] was utilized for the spring elements to connect the CNT layers. They mentioned that an increase in diameter may not lead to increase of the Young modulus of CNTs. Also, similar to Kalamkarov et al. [20], Li et al. [22] studied the mechanical behavior of CNTs and found that chirality had no impact on the Young modulus of MWCNTs and it could be increased by adding layers. Liew et al. [23] used the molecular dynamic technique and the second-generation Brenner potential [8], to mention that the Young modulus was decreased by increase of layers. Tu et al. [24] assumed that the total energy could be considered as sum of the bonding and nonbonding energies and derived the Young modulus for

MWCNTs based on the Young modulus of SWCNTs. They proved that Young modulus decreases by increase of walls but if the wall exceeds 100, the Young modulus remains fixed. Mohammadpour et al. [25, 26] used the Morse potential [27] and the spring elements to connect the layers and they found that the Young modulus increases by number of layers in single, double, and three walled CNTs.

In the present research, to simulate the mechanical behavior of SWCNT and MWCNT the energy-stretch curve of a C-C bond was computed in the tension and compression by means of the second-generation Brenner potential [8]. The material parameters of the C-C bond were obtained by simultaneous fitting of the tension-compression results to the Ogden [15], Moony-Rivlin [28], and Yeoh [29] hyperelastic models. The best model was selected according to the fit quality and the material stability of the basic loading modes. Based on the selected hyperelastic model, the SWCNT was simulated in ABAQUS. Finally, the mechanical behavior of MWCNTs was predicted using the hyperelastic model and the spring elements as a tool for connecting the walls. The spring stiffness was determined from the second derivative of the Lennard-Jones potential [21].

2. Simulation of SWCNT and MWCNT

The SWCNTs and MWCNTs were created by cylindrical arrangement of the graphene plate from the hexagonal structures with covalent bonds. The main characteristic of these covalent bonds are length and bond angle that are considered as 1.42 Å and 120°, respectively. Using the geometric similarity of CNTs to the space-frame structure in nano-scale continuum model, the covalent bond is considered as the beam element with the diameter of 1.47 Å [25, 26]. The structure of SWCNT was assumed as similar to that of Fig. 1 in simulations [25, 26] and the geometry of MWCNTs (without Van der Waals bonds) could be seen in Fig. 2.

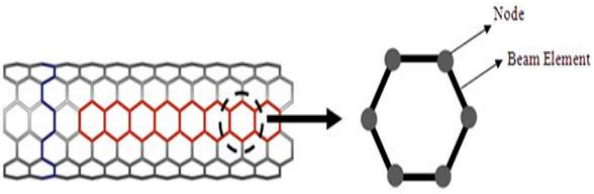

Fig. 1. Hexagonal structure of a typical SWCNT [25, 26].

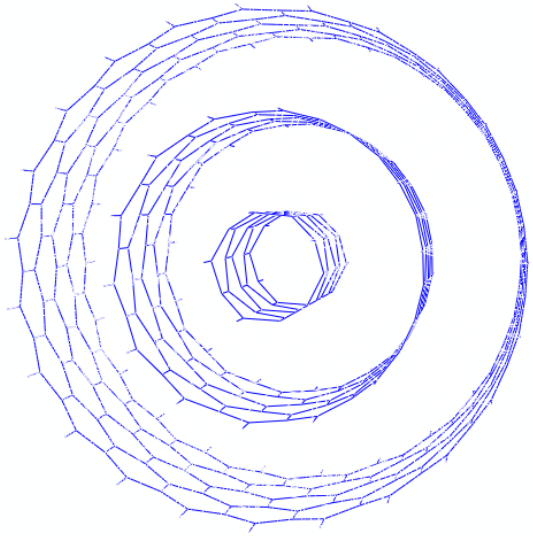

Fig. 2. Front view of three wall CNT.

In order to use the spring element between different layers, the Lennard-Jones potential function [21] was employed:

$$U_r = 4\varepsilon\left[\left(\frac{\sigma}{r}\right)^{12} - \left(\frac{\sigma}{r}\right)^{6}\right] \qquad (1)$$

in which ε and σ denote the Lennard-Jones parameters [21] and are considered as 0.002310 eV and 3.4 Å respectively. The equivalent spring stiffness ($K(r_{ij})$) can be extracted by the second derivative of Eq. (1) as:

$$F\left(r_{ij}\right) = \frac{dE_{ij}^{\,\mathrm{LJ}}}{dr_{ij}} = 24\frac{\varepsilon}{\sigma}\left[\left(\frac{\sigma}{r_{ij}}\right)^{7} - 2\left(\frac{\sigma}{r_{ij}}\right)^{13}\right] \qquad (2)$$

$$K(r_{ij}) = dF(r_{ij})/(dr_{ij}) = 24\frac{\varepsilon}{\sigma^2}\left[-7\left(\frac{\sigma}{r_{ij}}\right)^{8} + 26\left(\frac{\sigma}{r_{ij}}\right)^{14}\right] \qquad (3)$$

here $F\left(r_{ij}\right)$, $K(r_{ij})$, and r_{ij} denote the Lennard-Jones force, spring stiffness, and the distance between two atoms *i* and *j* [21]. The variation of spring stiffness with

respect to the interatomic distance was presented in Fig. 3. As it could be seen, when the distance between two atoms is greater than 4 Å, the spring stiffness approaches zero. Thereby, in the current research, spring element was created between the nodes with a distance greater than 3.3 Å and smaller than 4 Å. In Fig. 4, the cross section of the five walled CNT with spring elements that connected different walls of MWCNTs, is observed.

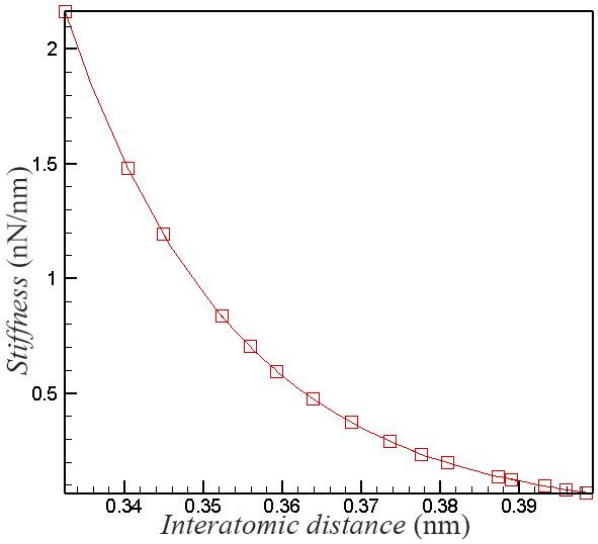

Fig. 3. Variation of the stiffness of structural spring with interatomic distance.

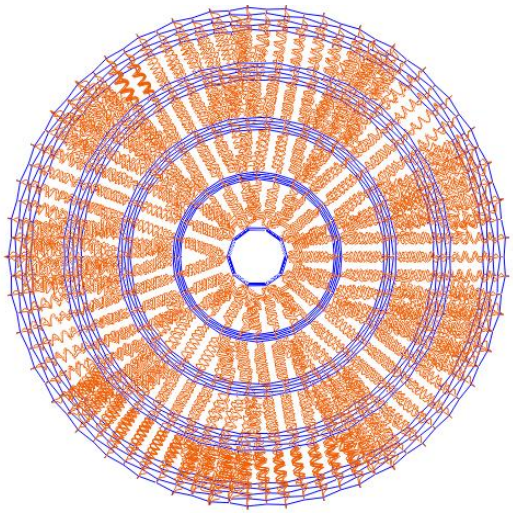

Fig. 4. Five walls CNT with spring element.

It is important to use an appropriate potential function that is able to describe the C-C covalent bonds in CNTs. The second-generation Brenner potential [8], which can describe formation and breaking of bonds, was employed as:

$$V\left(\mathrm{r_{ij}}\right)=V_{\mathrm{R}}\left(\mathrm{r_{ij}}\right)-\mathrm{B_{ij}}V_{\mathrm{A}}\left(\mathrm{r_{ij}}\right) \tag{4}$$

where $V_{\mathrm{R}}(\mathrm{ij})$ and $V_{\mathrm{A}}(\mathrm{ij})$ denote the attraction and repulsion potentials, respectively. Also, $\mathrm{B_{ij}}$ denotes the bond order that with respect to position of neighbor atoms, amplifies or weakens the attraction force versus repulsion force. The cut-off radius function, that is one for the closest neighbor atoms and is zero for the secondary neighbor atoms, could be mentioned as [8]:

$$f_c(r_{ij})=\begin{cases}1 & \mathrm{r_{ij}}<\mathrm{R^{(1)}}_{ij}\\ \frac{1}{2}-\frac{1}{2}\sin\left[\frac{\pi\left(r_{ij}-R_{ij}\right)}{\left(R^2_{ij}-\mathrm{R}^1_{ij}\right)}\right] & \mathrm{R^{(1)}}_{ij}<\mathrm{r_{ij}}<\mathrm{R^{(2)}}_{ij}\\ 0 & \mathrm{r_{ij}}>\mathrm{R^{(2)}}_{ij}\end{cases} \tag{5}$$

where $R^{(1)}_{ij}$ and $R^{(2)}_{ij}$ are 1.7 and 2 Å, respectively [8]. The following attraction and repulsion potentials were used [8]:

$$V_{\mathrm{R}}\left(\mathrm{r}_{ij}\right)=\frac{\mathrm{D^{(e)}}}{\mathrm{S}-1}\mathrm{e}^{\sqrt{2\mathrm{S}}\left(-\beta\left(r_{ij}-\mathrm{R^{(e)}}\right)\right)}f_c\left(\mathrm{r}_{ij}\right) \tag{6}$$

$$V_{\mathrm{A}}\left(\mathrm{r}_{ij}\right)=\frac{\mathrm{D^{(e)}S}}{\mathrm{S}-1}\mathrm{e}^{\sqrt{\frac{2}{\mathrm{S}}}\left(-\beta\left(r_{ij}-\mathrm{R^{(e)}}\right)\right)}f_c\left(\mathrm{r}_{ij}\right) \tag{7}$$

where parameters $\mathrm{D^{(e)}}$, S, and β were obtained from references [8]. $\mathrm{R^{(e)}}$ shows the length of the equilibrium bond between two carbon atoms and is equal to 1.42 Å [8]. Inspecting Eqs. 4 to 7 reveals it is possible to find variation of the energy versus the bond length (r_{ij}). This change in bond length in this research is considered to be caused due to the deformation.

3. Hyperelastic Models

In the current research the Ogden [15], Mooney-Rivlin [28], and Yeoh [29] models were considered to describe the mechanical behavior of the C-C bond at large strains. For the sake of reference to these equations, they were defined in Eqs. (8) to (10), respectively:

$$W=\sum_{i=1}^{N}\frac{2C_i}{\alpha_i^2}\left(\lambda_1^{\alpha_i}+\lambda_2^{\alpha_i}+\lambda_3^{\alpha_i}-3\right) \quad (8)$$

$$W=C_1\left(I_1-3\right)+C_2\left(I_2-3\right) \quad (9)$$

$$W=\sum_{i=1}^{3}C_i\left(I_1-3\right) \quad (10)$$

In these equations, α_i and C_i denote the material parameters and N is number of parameters, I_1 and I_2 are the first and second invariants of the right Cauchy-Green deformation tensor, λ_1, λ_2 and λ_3 are the principal stretches. If the uniaxial deformation mode is considered ($\lambda_1=\lambda_2^{-0.5}=\lambda_3^{-0.5}$), it is easily could be shown that the $\sum_{i=1}^{N}C_i$ is equal to shear modulus and the Young modulus (E) could be expressed as Eq. (11):

$$\sum_{i=1}^{N}C_i=\frac{E}{3} \quad (11)$$

Thereby, the Young modulus of the CNTs could be calculated when the hyperelastic material parameters were determined.

4. Hyperelastic Material Parameters

Although materials possess different stress-strain (or stretch) curves under different loading conditions, they have the same energy-strain function under all loading modes [19] and thereby we found the hyperelastic material parameters by energy-stretch curve. In general, the nonlinear optimization techniques should be adapted for the material parameters definition [30]. Here, the following error was defined that should be minimized [19].

$$error=\frac{\left\|W_{\text{model}}-W_{\text{data}}\right\|_{L_2}}{\left\|W_{\text{data}}\right\|_{L_2}} \quad (12)$$

where W_{data}, W_{model}, and L_2 denote the energy of the second-generation Brenner potential, the hyperelastic strain energy function, and the Euclidian norm [19]. In order to determine W_{data} a unit cell that shows the behavior of a C-C bond, its neighbors in the hexagonal structure of graphene was considered (Fig. 5). Then, it was subjected to tension and compression and the energy-stretch curve was determined from the second-generation Brenner potential (REBO) [8] in the compression and tension. The energy-stretch curve of the unit cell and the results of Flores et al. [16] that extracted from the Material Studio software could be seen in Fig. 6. As illustrated, the results of the current implementation of REBO model is in agreement with the results of commercial software of Material Studio. The energy data of Fig. 6 was considered as W_{data} in Eq. (12).

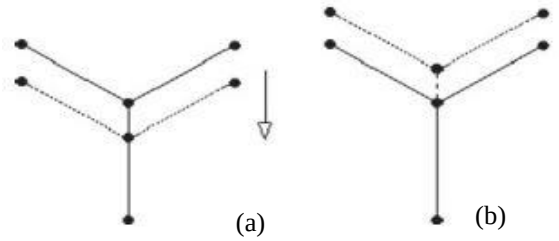

Fig. 5. C-C bond unit cell under: a) compression and b) tension [16].

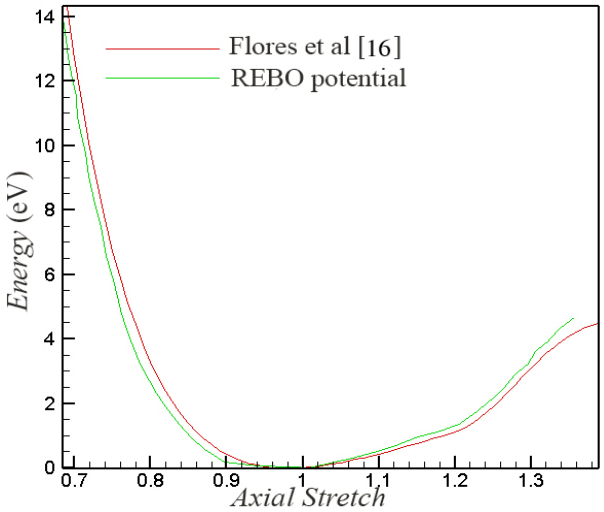

Fig. 6. Comparison of second-generation Brenner potential curve with results of Flores et al. [9].

Fitting the uniaxial energy of the unit cell (Fig. 6) to the hyperelastic strain energy functions provides the material parameters of each model. To this end, the error defined by Eq. (12) was minimized in MATLAB software by using the Fminimax function.

5. Tension of SWCNT

In the present study, for the purpose of comparing our predictions to the results obtained by Flores et al [16], the SWCNT with chirality of (7, 7) with 574 nodes and 847 elements was considered. The same boundary conditions as Flores et al. [9] were imposed to the ends of CNT, as seen in Fig. 7. In order to consider the transverse deformation, the Timoshenko beam was employed and hybrid element was utilized due to the incompressible nature of bonds (material incompressibility). The length of C-C bond and equivalent bond diameter were assumed as 0.142 nm and 0.147 nm, respectively [8, 17].

6. Results and Discussion

6.1. Results of tensile loadings on SWCNT

As previously mentioned, the tension and compression response of the nonlinear elastic materials may be different and for the C-C bond it is evident in Fig. 6. Hence, in the present study we consider both tension and compression to determine the material parameters. The material parameters and the fitting error (according to Eq. 12) of the studied hyperelastic models could be seen in table 1.

The results of the curve fitting of the Yeoh, Moony-Rivlin, first and second order Ogden models to the second-generation Brenner potential, as well as the predicted stress-strain curves for the mentioned models could be seen in Fig. 8.

As shown in Fig. 8(a) the fitting quality is not reasonable for the Yeoh model although from Fig. 8(b) the stable material behavior could be seen in all basic deformation modes including the uniaxial (tension and compression), balanced biaxial tension, and shear. From Fig. 8(d), the Moony-Rivlin model represents the material instability in tension and thereby it could not be used for the investigation of the mechanical behavior of CNTs while a better fitting could be seen in Fig. 8(c) than Fig. 8(a). Based on Figs. 8(e) and 8(f), it is observed that the first order Ogden model represents both of the material stability and reasonable fit. However, in order to increase the fitting quality, the second order Ogden model was also used and from Fig. 8(g) both the best fitting quality as well as the material stable behavior could be seen (Fig. 8(h)).

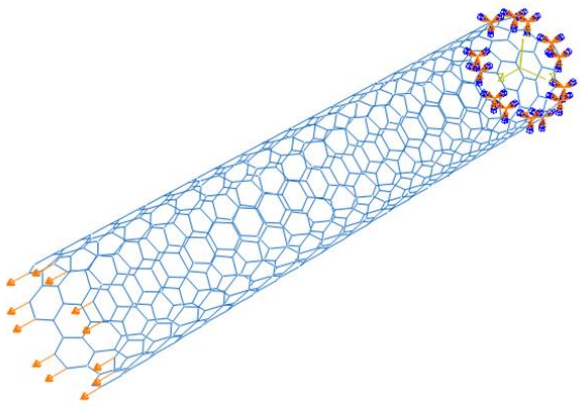

Fig. 7. Tensile boundary conditions on SWCNT.

Table 1. Material parameters of hyperelastic models for C-C bond

Model	Error (%)	C_1(GPa)	C_2(GPa)	C_3(GPa)	α_1	α_2
Yeoh	18	844.47	1845.1	400.07	-	-
Moony-Rivlin	1.2	-1837.5	3230.4	-	-	-
First order Ogden	0.22	2147.7	-	-	-6.8983	-
Second order Ogden	0.12	1786.5	154.95	-	-7.9521	9.5711

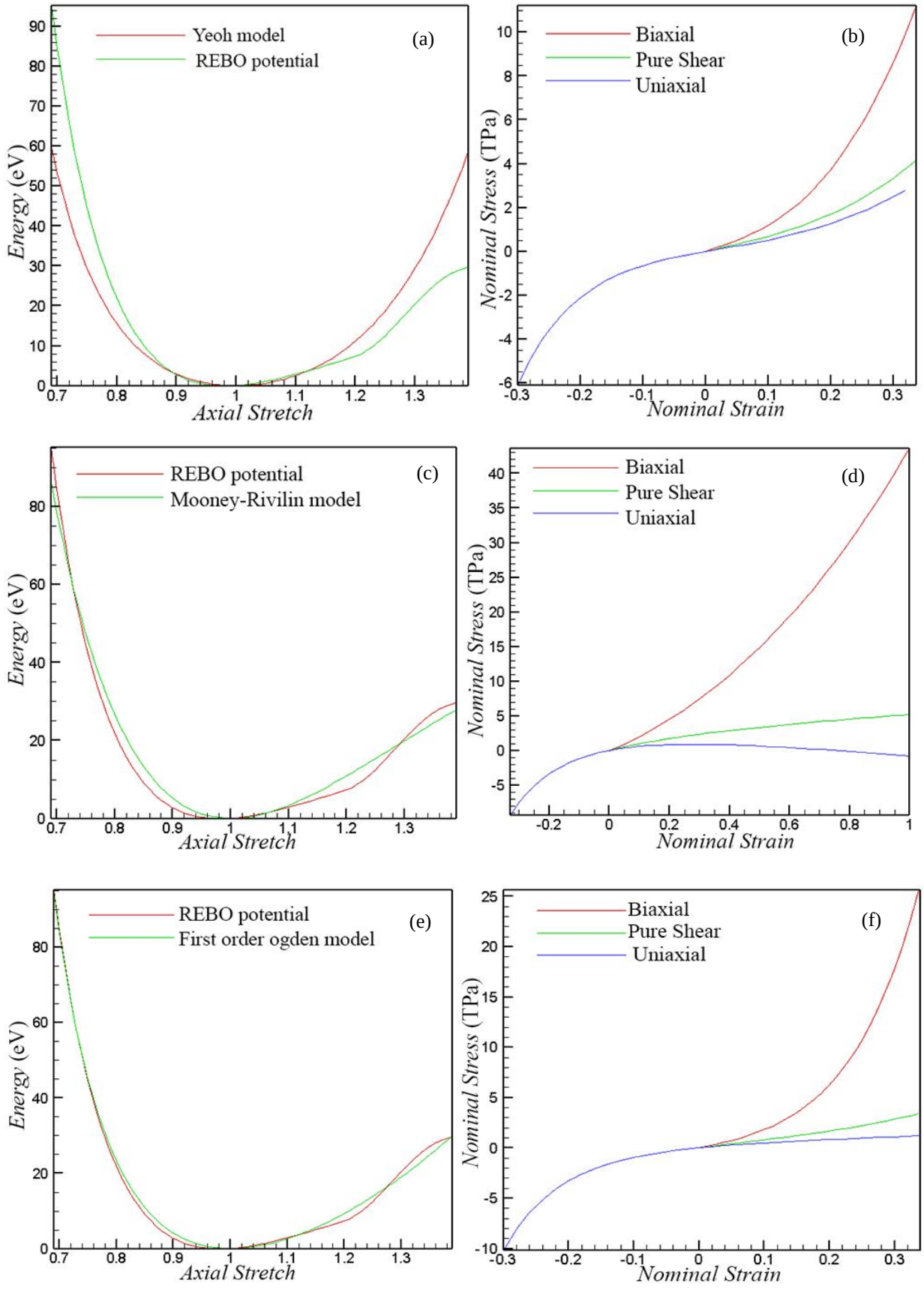

Fig. 8. Comparison of the second-generation Brenner potential [8] and, (a, c, e, g) different hyperelastic models and (b, d, f, h) stress-strain response of hyperelastic models.

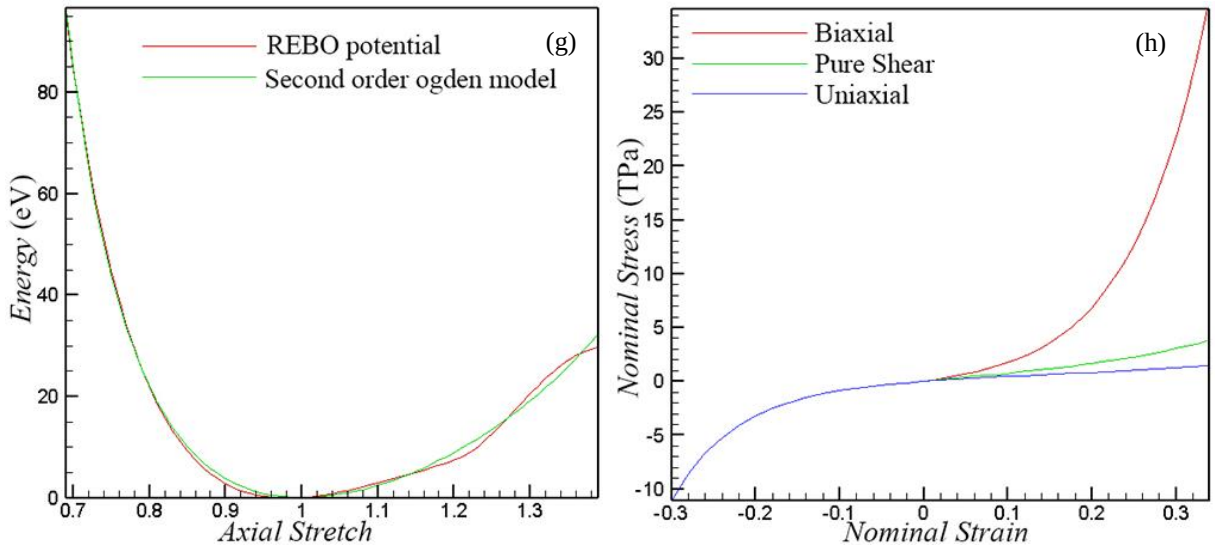

Fig. 8. Continue.

It is worth to mention that Flores et al. [16] introduced two sets of material parameters where one which was derived from the tension part of Fig. 6 and another from the compression part of this figure (table 2); with an expectation of unique material parameters. We simulated the tension behavior of SWCNT (7, 7) with these two sets of material parameters and the results could be seen in Fig. 9.

Table 2. Material parameters (constants) of the first order Ogden model from Flores et al. [16]

	α	C (*GPa*)
Tensile part of Fig. 6	-14	2332.36
Compression part of Fig. 6	-10	1166.18

It could be seen from Fig. 9 that by taking into consideration two sets of material parameters, a unique response in tension could not be achieved and the difference between the results increases by increasing deformation. Therefore, although the results of tension loading, according to the material parameters from tension part of Fig. 6, is acceptable but for more complicated loadings like buckling and bending it is not clear which set of material parameters should be used. Meanwhile, as it was seen in the current research, a unique set of material parameters was derived by simultaneously considering both of the tension and compression. Accordingly, the CNT of Fig. 7 was simulated and the results of reaction force for the Yeoh and second order Ogden models could be seen in Fig. 10. As illustrated, the second order Ogden model represents a good agreement with the results of Flores et al. [9]; despite the fact that their results were provided by the material parameters from the tensile part of Fig. 6 and our material parameters consider both loading modes. From Figs. 8(g) and 10 it could be concluded that the second order Ogden model not only describes the CNT mechanical behavior but it could also be used as the material property of the C-C bond.

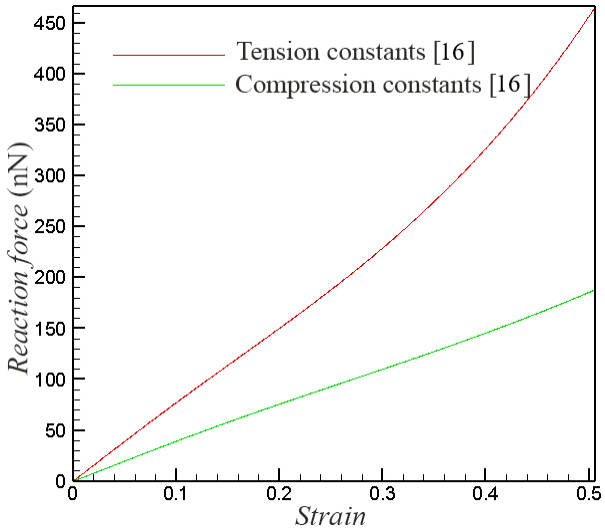

Fig. 9. Tension behavior of SWCNT (7, 7) with material parameters of reference [9].

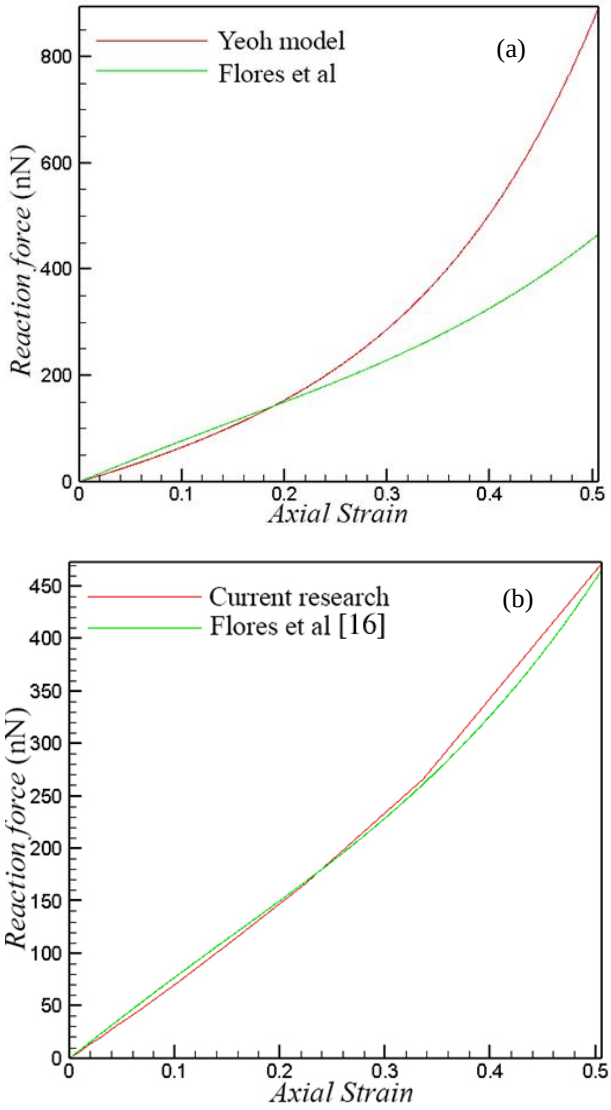

Fig. 10. Tension loading from simultanous tension-compression parameters, (a) Yeoh and (b) second order Ogden models.

From Fig. 6 the breaking (fracture) strain of C-C bond in tension could be estimated as 0.33 [9] where a maximum in the curve could be seen. From the strain contour of the deformed SWCNT in Fig. 11 the elements with the strain 0.33 were indicated where the failure of SWCNT starts from these points and leads to non-uniform and irreversible deformation.

In the buckling and bending of CNTs, some parts of structure is under tension while others are under compression. Accordingly, the transverse bending of (20, 0) SWCNT with length of 10 nm was simulated by the material parameters of table 2 (Liang et al. [11]) and the second order Ogden model presented in table 1 (current research). To this end, the CNT was subjected to transverse bending (Fig. 12) and the resultant maximum normal stress versus deflection was presented in Fig. 13.

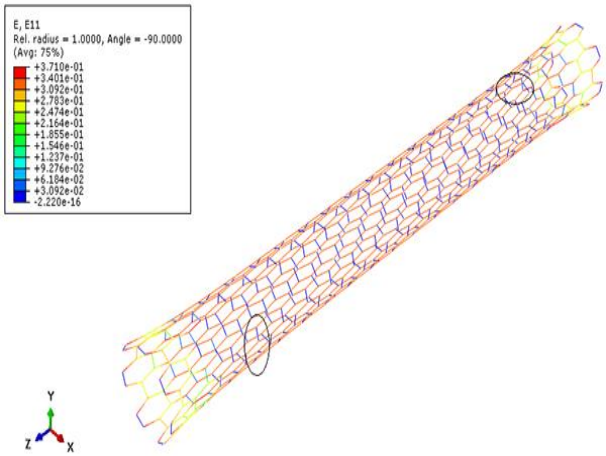

Fig. 11. Deformed contour of SWCNT in tension.

In the buckling and bending of CNTs, some parts of structure is under tension while others are under compression. Accordingly, the transverse bending of (20, 0) SWCNT with length of 10 nm was simulated by the material parameters of table 2 (Liang et al. [11]) and the second order Ogden model presented in table 1 (current research). To this end, the CNT was subjected to transverse bending (Fig. 12) and the resultant maximum normal stress versus deflection was presented in Fig. 13.

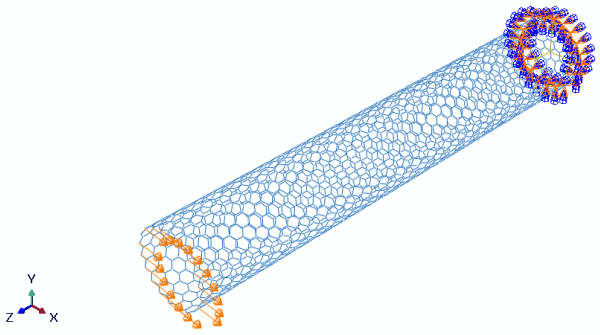

Fig. 12. Applied boundary condition of bending loading on SWCNT.

Figure 13 indicates that each set of the material parameters predicts different behavior. Taking into account that in bending one side of CNT is subjected to the tension and the other side is under compression, the use of the material parameters that derived from the tension or compression alone could not accurately predict the CNT mechanical behavior. Also, as it could be seen from Fig. 13, a good agreement between the results of the current research and MD simulation by Liang et al. on the same SWCNT could be achieved [11]. The slight difference may be due to the REBO and AIREBO potential functions which in the current and Liang et al. [11] research have been used, respectively. Fig. 14 exhibits the axial strain contour of the CNT in bending and the presence of tension (positive) and compression (negative) could be easily observed.

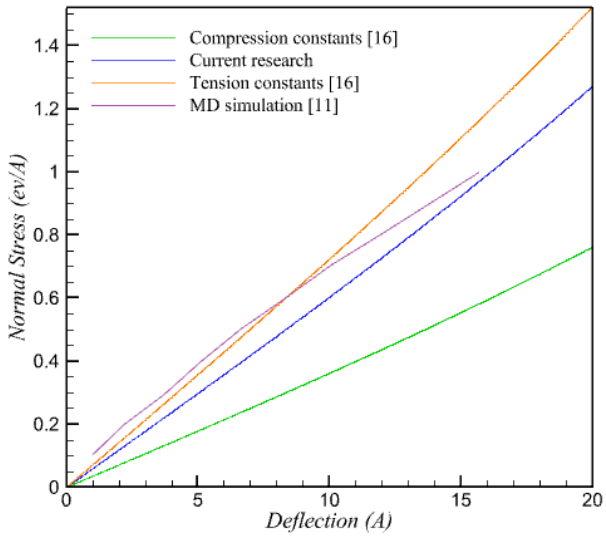

Fig. 13. Bending behavior of SWCNT with different tension and compression constants of Flores et al. and from current research.

6.2. Tension of MWCNTs

To predict the mechanical behavior of MWCNTs, different chirality was considered (table 3). Spring elements were used to connect the walls, as shown in Fig. 4.

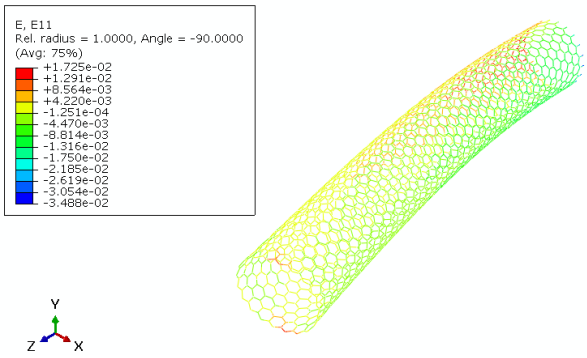

Fig. 14. Deformed SWCNT under bending.

Table 3. Characterization of MWCNTs in current research

CNTs	Chirality of walls
SWCNT	(5,0)
Double wall	(5,0), (14,0)
Triple wall	(5,0), (14,0), (23,0)
Quadruple wall	(5,0), (14,0), (23,0), (32,0)
Quintuple wall	(5,0), (14,0), (23,0), (32,0), (41,0)
Sextuple wall	(5,0), (14,0), (23,0), (32,0), (41,0), (50,0)
Septuple wall	(5,0), (14,0), (23,0), (32,0), (41,0), (50,0), (59,0)
Octuple wall	(5,0), (14,0), (23,0), (32,0), (41,0), (50,0), (59,0), (68,0)

To implement boundary conditions similar to Fig. 15, the degrees of freedom of all walls were constrained at one end and only the most external wall of the other side was subjected to the loading as the outmost layer of MWCNT is touched by the atomic force microscope (AFM) and the other layers slip by the well-known telescopic mechanism [31].

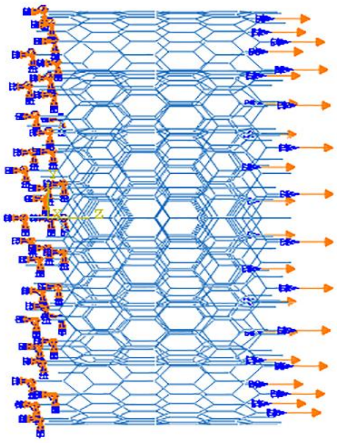

Fig. 15. Different views of applied boundary conditions for tension loading on quadruple (four) walls CNT.

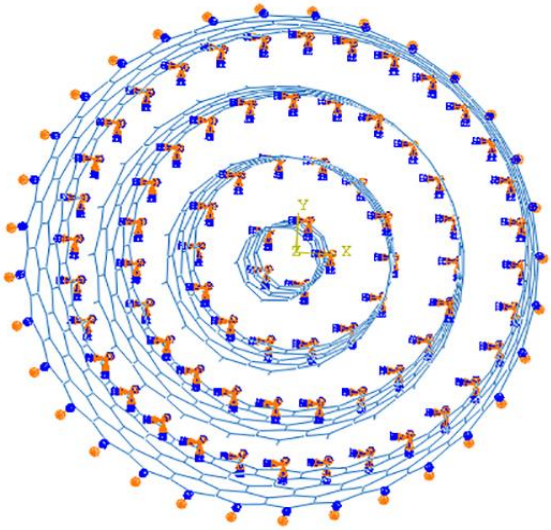

Fig. 15. Continue.

The reaction force, due to the imposed displacement, was computed at the loading edge and Eq. (13) was employed to compute the stress [22].

$$S = \frac{F}{A} \tag{13}$$

here F and A denote the reaction force and surface area of CNT. The surface area of cross section of SWCNTs and MWCNTs could be calculated, respectively, by the following equations [22]:

$$\mathrm{A}_{SWCNT} = \pi\left[\left(R_{NT} + \frac{t}{2}\right)^2 - \left(R_{NT} - \frac{t}{2}\right)^2\right] \tag{14}$$

$$\mathrm{A}_{MWCNT} = \pi\left[\left(R_{NT,out} + t\right)^2 - \left(R_{NT,in} - t\right)^2\right] \tag{15}$$

where R_{NT} denotes the radius of SWCNT, $R_{NT,in}$ and $R_{NT,out}$ are the internal and external radii of MWCNT, respectively. In the above equations, t expresses the thickness and it is equal to the space between graphite sheets (3.4 Å). The cross section of the various types of CNTs could be seen in Fig. 16 from the atomistic and continuum viewpoints [20]. The predicted reaction force-strain and stress-strain curves were shown for the assumed CNTs of table 3 in Fig. 17, in tension and compression.

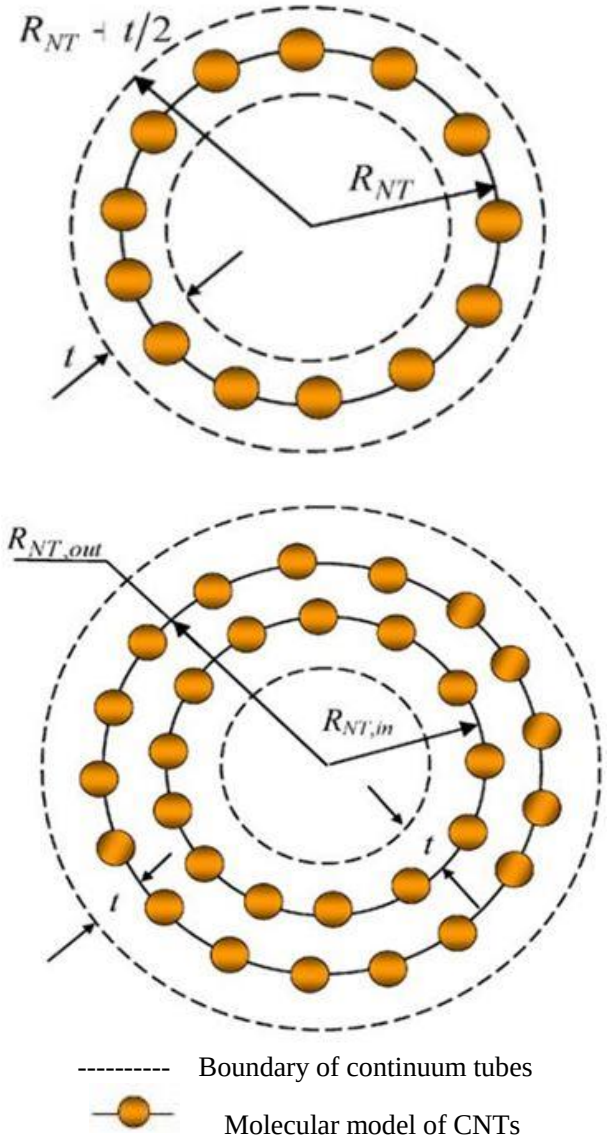

Fig. 16. cross section of CNTs and their continuum tube models, (a) SWCNT and (b) MWCNTs [20].

Figure 17 indicates that by increasing the walls leads to a raise in the reaction forces; this is due to the increase of the C-C bonds. However, Fig. 17 (b) represents the stress reduction caused by increasing the walls because a rise in the diameter causes an increase in the surface area and therefore, leading to stress reduction according to Eq. (13). Moreover, the weak Van der Waals bonds between the layers lead to difficult transfer of the imposed load on the external layer to the internal layers and the they slip over each other without noticeable deformation (telescopic mechanism).

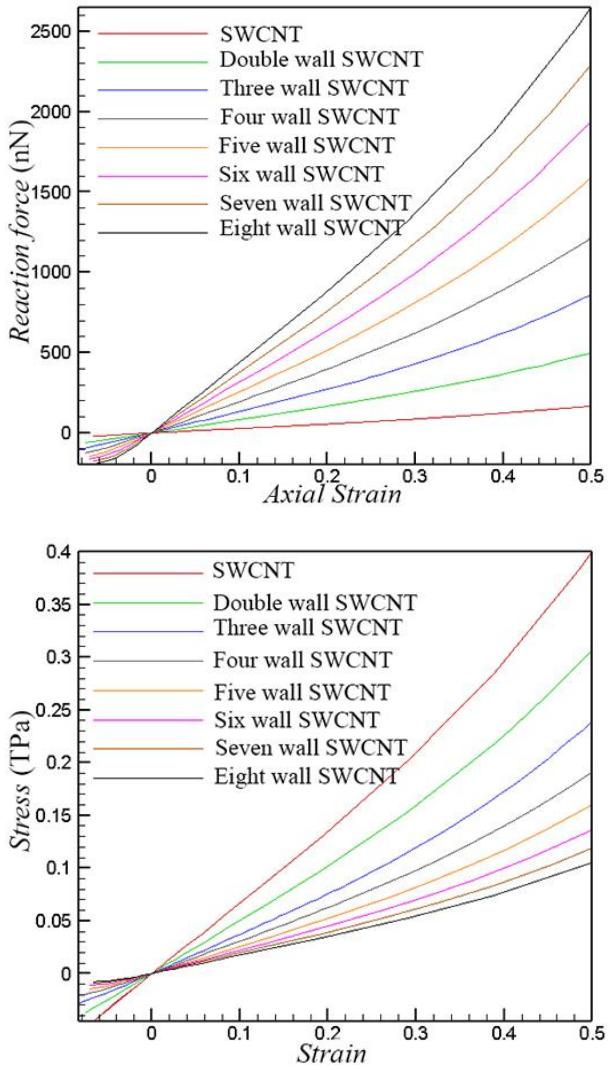

Fig. 17. Loading of MWCNTs, (a) reaction force-strain and (b) stress-strain.

As it was mentioned, the material parameters of table 1 presented for the C-C bond that constructs an element of CNTs. Fig. 17 depicts the nonlinear behavior of MWCNTs. Here, for the first time, the material parameters of the hyperelastic response of MWCNTs were determined. To achieve this goal, the stress-strain of each MWCNT in Fig. 17 (considering the tension and compression simultaneously) was fitted to the first order Ogden hyperelastic model and the computed material parameters could be observed in table 4. From Eq. (11), the Young modulus of the MWCNTs was determined and the results, as a function of layer numbers, could be seen in Fig. 18.

Table 4. Material parameters of the first order Ogden model of MWCNT.

CNTs	$C_1(TPa)$	α_1
SWCNT	0.224	4.66
Double wall	0.167	4.79
Triple wall	0.120	5.12
Quadruple wall	0.097	5.17
Quintuple wall	0.081	5.19
Sextuple wall	0.070	5.18
Septuple wall	0.060	5.29
Octuple wall	0.054	5.23

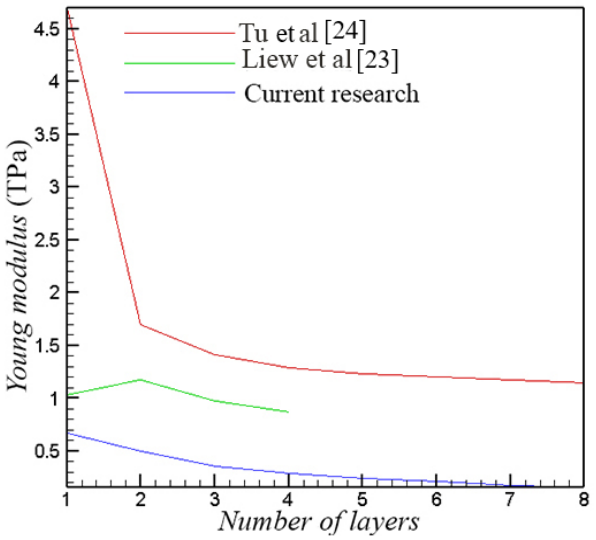

Fig. 18. Variation of the Young modulus with the number of MWCNT layers.

Figure 18 shows the Young modulus decreases with an increase in layer numbers and the trend of the current research is consistent with the results of molecular dynamic by Liew et al. [23] and linear elasticity by Tu et al. [24]. This is noteworthy given that it could be seen in Fig. 18 that the Young modulus of MWCNT is smaller than the Young modulus of SWCNT when the load is imposed on the external layer of CNT. One of the reasons for these differences between our results with Liew et al. [23] is the distance between layers (distance between layers is equal to thickness of layers). In the

research of the Liew et al. [23], distance between layers raises by increasing them (3.35 and 13.4 Å for SWCNT and four wall CNTs respectively). Therefore, increasing thickness, according to Eq. (15), leads to an increase in the cross-section area and, according to Eq. (13), a decrease in the stress. But, in the current research, the thickness was assumed to be fixed for all CNTs [16, 25, 26]. Moreover, in the research of Tu et al. [24], Young's modulus of MWCNTs (Y_m) was obtained in terms of the Young's modulus of the SWCNT (Y) based on the following simplified analytical equation.

$$Y_m = \frac{N}{N - 1 + h/d}\frac{h}{d}Y \tag{16}$$

here, N, h, and d denote the number of layers, effective wall thickness (0.75 Å) and distance between layers (3.4 Å). But, in our research, the Young modulus was obtained according to the simulation of MWCNTs which is more realistic. It is worth noting that in our research, similar to Mohammadpour et al. [25, 26] and Flores et al. [16], the distance between the layers and the thickness of the layers were assumed to be 3.4 Å.

Mohammadpour et al. [25, 26] simulated MWCNTs where all layers were subjected to the tensile loading. We simulated the same MWCNTs and the tensile load was applied on all layers of MWCNT. Then the Young's modulus of simulated MWCNTs was determined (see table 5).

Table 5. Comparison of the Young's modulus of MWCNTs with the results of Mohammadpour et al.

Young's modulus (TPa)		
MWCNTs	Current research	Mohammadpour et al. [25, 26]
(5,0), (14,0)	0.675	0.9512
(5,0), (14,0), (23,0)	1.483	0.9724

From table 5 it could be concluded that when the load is applied to all layers, the Young modulus raises by increasing the layers because of the contribution of the total number of SWCNT layers that constitute the MWCNTs. However, difference between the results of the two studies could be related to the second-generation Brenner potential of the current research while the Morse potential function [27] has been used by Mohammadpour et al. [25, 26] and it is consistent with the second-generation Brenner potential up to a strain of 0.01. Additionally, in the research of Mohammadpour et al. [25, 26], the linear elasticity has been used while according to Fig. 17 the nonlinear elasticity was considered in the current study. It noteworthy that in real experiments of CNTs only the external layer is touched by the loading tip of the atomic force microscopy and thereby we considered this fact in our simulations.

7. Conclusions

The material parameters of Ogden [32], Moony-Rivlin [31], and Yeoh [27] hyperelastic models were derived in order to fit the tension and compression of the C-C bond in a unit cell. These constants were used to predict the mechanical behavior of armchair SWCNT in tension. The results of simulations indicated that the second order Ogden model could describe the hyperelastic behavior of CNTs for the tension and compression loading modes. In addition, the strain contours of the SWCNT simulation determined the failure location when the bond (element) reaches the critical strain of C-C bond. Considering hyperelastic material parameters of C-C bond, the MWCNTs were simulated by connecting layers with spring elements that have their stiffness derived from the Lennard-Jones potential and the loading was imposed to the external layer. Results showed that stress-strain curves approach each other with an increase in layer numbers. By fitting the predicted stress-strain curves of MWCNTs, the material parameters of the first order Ogden hyperelastic model were obtained. Finally, the Young modulus of MWCNTs was determined and it was observed that it decreases when there is an increase in the layers because of how internal layers slip on each other (telescopic mechanism).

8. Acknowledgment

The authors would like to thank the K. N. Toosi University of Technology, Tehran, Iran, for the financial support and research facilities used in this work.

9. References

[1] N.A. Sakharova, A.F.G. Pereira, J.M. Antunes, C.M.A. Brett, J.V. Fernandes, Mechanical characterization of single-walled carbon nanotubes: Numerical simulation study, *Composites Part B: Engineering*, 75 (2015) 73-85.

[2] X. Gui, J. Wei, K. Wang, A. Cao, H. Zhu, Y. Jia, Q. Shu, D. Wu, Carbon nanotube sponges, *Advanced materials*, 22 (2010) 617-621.

[3] X. Gui, H. Li, K. Wang, J. Wei, Y. Jia, Z. Li, L. Fan, A. Cao, H. Zhu, Dehai Wu, Recyclable carbon nanotube sponges for oil absorption, *Acta Materialia*, 59 (2011) 4798- 4804.

[4] A. Pantano, D. M.Parks, M. C.Boyce, Mechanics of deformation of single- and multi-wall carbon nanotubes, *Journal of the Mechanics and Physics of Solids*, 52 (2004) 789-821.

[5] R. Rafiee, R.M. Moghadam, On the modeling of carbon nanotubes: a critical review, *Composites Part B: Engineering*, 56 (2014) 435-449.

[6] K.I. Tserpes, P. Papanikos, Finite element modeling of single-walled carbon nanotubes, *Composites Part B: Engineering*, 36 (2005) 468-477.

[7] T. Xiao, K. Liao, Nonlinear elastic properties of carbon nanotubes subjected to large axial deformations, *Physical Review B*, 66 (2002) 153407 (1-4).

[8] D. W. Brenner, O. A. Shenderova, J. A., Harrison, S. J. Stuart, S. B. Sinnott. A second-generation reactive empirical bond order (REBO) potential energy expression for hydrocarbons, Journal of Physics: Condensed Matter, 14 (2002) 783-802.

[9] B. WenXing, Z. ChangChun, Cui WanZhao, Simulation of Young's modulus of single-walled carbon nanotubes by molecular dynamics, *Physica B*, 352 (2004) 156-163.

[10] K. G. S. Dilrukshi, M. A. N. Dewapriya, U. G. A. Puswewala, Size dependency and potential field influence on deriving mechanical properties of carbon nanotubes using molecular dynamics, *Theoretical and Applied Mechanics Letters*, 5 (2015), 167-172.

[11] Y. Liang, Q. Han, J. Ou, Bending Solutions of Cantilever Carbon Nanotubes and Molecular Dynamics Simulation, *Journal of Computational and Theoretical Nanoscience*, 11 (2014) 71-75.

[12] X. Ling, S.N. Atluri, A hyperelastic description of single wall carbon nanotubes at moderate strains and temperatures, *Computer Modeling in Engineering and Sciences*, 21 (2007) 81-91

[13] X. Ling, S. N. Atluri, hyperelastic description of single wall carbon nanotubes, *Journal of applied physics*, 101 (2007), 064316 (1-4).

[14] E. I. Saavedra Flores, S. Adhikari, M. I. Friswell, F. Scarpa, Hyperelastic modelling of post-buckling response in single wall carbon nanotubes under axial compression, *Procedia Engineering*, 10 (2011) 2256–2261.

[15] R.W. Ogden, Non-linear elastic deformations, *Courier Corporation*, 1997.

[16] E.I. Saavedra Flores, S. Adhikari, M.I. Friswell, F. Scarpa, Hyperelastic finite element model for single wall carbon nanotubes in tension, *Computational Materials Science*, 50 (2011) 1083-1087.

[17] D.W. Brenner, Empirical potential for hydrocarbons for use in simulating the chemical vapor deposition of diamond films. *Physical review B*, 42 (1990) 9458-9471.

[18] H. Darijani, R. Naghdabadi, Hyperelastic materials behavior modeling using consistent strain energy density functions, *Acta mechanica*, 213 (2010) 235-254.

[19] M. Hosseinzadeh, M. Ghoreishi, K. Narooei, Investigation of hyperelastic models for nonlinear elastic behavior of demineralized and deproteinized bovine cortical femur bone, *Journal of the mechanical behavior of biomedical materials*, 59 (2016) 393-403.

[20] A.L. Kalamkarov, A.V. Georgiades, S.K. Rokkam, V.P. Veedu, M.N. Ghasemi-Nejhad, Analytical and numerical techniques to predict carbon nanotubes properties, International *Journal of Solids and Structures*, 43 (2006) 6832-6854.

[21] P. S. Rao, S., Anandatheertha, G. N. Naik, S. Gopalakrishnan, Estimation of mechanical properties of single wall carbon nanotubes using molecular mechanics approach. Sadhana, 40 (2015) 1301-1311.

[22] C. Li, TW. Chou, Elastic moduli of multi-walled carbon nanotubes and the effect of van der Waals forces, *Composites Science and Technology*, 63 (2003) 1517- 1524.

[23] K. M. Liew, X. Q. He, C. H. Wong, On the study of elastic and plastic properties of multi walled carbon nanotubes under axial tension using molecular, *Acta Materialia*, 52 (2004) 2521-2527.

[24] Z. c. Tu, Z. c. Ou-Yang, Single-walled and multiwalled carbon nanotubes viewed as elastic tube with the effective Young's moduli dependent on layer number. *Physical Review B*, 65 (2002) 1-4.

[25] E. Mohammadpour, M. Awang. "Nonlinear finite-element modeling of graphene and single-and multi-walled carbon

nanotubes under axial tension. *Applied Physics A*, 106 (2012) 581-588.

[26] E. Mohammadpour, M. Awang, A finite element model for predicting the tensile behavior of carbon naotube, *2011 National Postgraduate Conference*, (2011) 1-6.

[27] J.R. Xiao, B.A. Gama, J.W. Gillespie Jr, An analytical molecular structural mechanics model for the mechanical properties of carbon nanotubes, *International Journal of Solids and Structures*, 42 (2005) 3075-3092.

[28] W. W. Feng, J. O. J. s. Hallquist, On Mooney-Rivlin constants for elastomers, *stress (force per unit undeformed area)*, 1 (2017) 1-10.

[29] C. Renaud, J. M. Cros, Z. Q. Feng, B. Yang, The Yeoh model applied to the modeling of large deformation contact/impact problems, *International Journal of Impact Engineering*, 36 (2009) 659-666.

[30] T. Beda, An approach for hyperelastic model-building and parameters estimation a review of constitutive models, *European Polymer Journal*, 50 (2014) 97-108.

[31] M. F. Yu, O. Lourie, M. J. Dyer, K. Moloni, T. F. Kelly, R.S. Ruoff, Strength and breaking mechanism of multiwalled carbon nanotubes under tensile load, *Science*, 287 (2000) 637-640.

رویکرد مکانیک ساختاری برای بررسی رفتار مکانیکی هایپرالاستیک نانولوله‌های کربنی تک جداره و چند جداره

معصومه رشیدی و کیوان نارویی

دانشکده مهندسی مواد و مواد، دانشگاه صنعتی خواجه نصیر الدین طوسی، تهران، ایران.

چکیـــده

در تحقیق حاضر به منظور پیشگویی رفتار هایپرالاستیک نانولوله‌های کربنی تک جداره و چند جداره از یک مدل المان محدود سه بعدی استفاده شد. با فرض رفتار الاستیک غیرخطی پیوند کربن- کربن در کرنش‌های بزرگ، مدل‌های هایپرالاستیک درنظر گرفته شدند. بررسی مقالات نشان داد اگرچه رفتار الاستیک غیرخطی در کشش و فشار یکسان نیست، اما پارامترهای مادی مدل‌های هایپرالاستیک در بارگذاری کشش تک محوره تعیین شده است. بدین ترتیب، منحنی انرژی- کشش پیوند کربن- کربن با استفاده از پتانسیل برنر نسل دوم در شرایط کشش و فشار تک محوره تعیین شد. نتایج بدست آمده با تابع‌های انرژی کرنش هایپرالاستیک آگدن، مونی- رایولین و یوه جهت بدست آوردن پارامترهای مادی مدل‌های مذکور انطباق داده شد. نتایج نشان داد که مدل آگدن مرتبه دوم می‌تواند رفتار کشش و فشار پیوندهای کربن- کربن را به طور دقیق توصیف کند. نتایج خمش نانولوله تک جداره نشان داد که با در نظر گرفتن پارامترهای مادی حاصل از داده‌های کشش و فشار به طور همزمان، می‌توان به یک پاسخ یکتا دست یافت. از نتایج نانولوله‌های تک جداره، رفتار مکانیکی نانولوله‌های چند جداره با فرض پیوندهای واندروالس ایجاد شده بین لایه‌های نانولوله‌های چند جداره با استفاده از پتانسیل لنارد-جونز، پیش بینی شد. نتایج بارگذاری روی لایه خارجی نانولوله‌های چند جداره نشان داد که افزایش لایه‌ها باعث کاهش تنش می‌شود به گونه‌ای که منحنی تنش-کرنش فراتر از ۸ لایه یکسان می‌شود. بر این اساس، پارامترهای مادی مدل آگدن مرتبه اول با درنظر گرفتن پاسخ همزمان کشش و فشار برای نانولوله‌های چند جداره تعیین شد.

واژه‌های کلیدی: نانولوله کربنی تک جداره، چند جداره، هایپرالاستیک، پتانسیل برنر، پتانسیل لنارد جونز